Quantum Computing With Trapped Ions

Riccardo Valperga

Department of Physics, Imperial College of Science, Technology and Medicine

Abstract

Since it has been demonstrated that a large-scale quantum computer (QC) could efficiently solve useful tasks that are classically intractable, trapped ions have remained one of the most promising technologies to realize such devices physically. This report is intended to be a review of the state of the art of trapped-ions quantum computers that can be programmed to implement quantum logic gates. In particular, before going through the physical realizations, the principles on which quantum computing is grounded are outlined from a theoretical point of view. After that, the way quantum logic gates are performed on these devices is described.

Contents

1 Quantum Gates

The idea that quantum mechanical effects can be harnessed to change the nature of computation profoundly appeared in 1985, in a paper by David Deutsch [1]. In this paper, Deutsch shows that the time required to solve a specific problem could depend on the physical apparatus used to perform the computation so that problems that have no polynomial-time solution can be solved by quantum computers in polynomial time.

By saying a polynomial-time solution, one means that the number of steps required to solve the problem is a polynomial function of the size of the problem.

A classical computer carries out computations using bits as basic units of information. The bits are physically represented by classical-behaving properties of a system, and therefore, during a computation, they are always in a defined state. The idea of a quantum computer is

that instead of using bits, the basic unit of information is represented by a two-level quantum mechanical system: the qubit. Suppose $|0\rangle$ and $|1\rangle$ form an orthonormal basis for the two-dimensional state space of this quantum mechanical system. Any arbitrary state vector can be written as

$$|\Psi\rangle = a|0\rangle + b|1\rangle \tag{1}$$

A QC uses two or more qubits to carry out computations, and it turns out [2] that the state of a quantum computer can be described as an entangled wave function living in a state space spanned by the tensor product of the basis states of the single qubits, e.g., for a two a qubits quantum computer:

$$\sum_{i,j=0}^{1} c_{ij} |i\rangle \otimes |j\rangle \tag{2}$$

Quantum mechanics tells us that as long as the state of the QC is not measured, it exists simultaneously in all of the states of which its wave function is the superposition. There are many well known two-level quantum mechanical systems that can be used to implement a qubit, in particular, in the experiments reported in this paper, the two-level system is realized by two of the electronic energy levels of ions confined in radiofrequency traps.

Like its classical counterpart, a quantum algorithm is made of fundamental operations, denoted quantum gates in analogy with the logic gates performed by classical computers on bits. Quantum gates are performed on a qubit register (i.e., a set of qubits) initialized at will (usually quantum algorithms are performed starting from a set of qubits in the +1 eigenstate with respect to the Z Pauli matrix of the two-level system). According to quantum mechanics postulates, any allowable transformation is a unitary transformation, represented by a 2x2 unitary matrix, that describes the time evolution of the input quantum state. Among the single-qubit gates, some of the most important are the Pauli matrices (X,Y, Z and $\mathbb{1}$), the Hadamard gate (H), the phase gate (S) and the $\pi/8$ gate (T):

$$X = \begin{bmatrix} 0 & 1 \\ 1 & 0 \end{bmatrix}; Y = \begin{bmatrix} 0 & -i \\ i & 0 \end{bmatrix}; Z = \begin{bmatrix} 1 & 0 \\ 0 & -1 \end{bmatrix} \tag{3}$$

$$H = \frac{1}{\sqrt{2}} \begin{bmatrix} 1 & 1 \\ 1 & -1 \end{bmatrix}; S = \begin{bmatrix} 1 & 0 \\ 0 & i \end{bmatrix}; T = \begin{bmatrix} 1 & 0 \\ 0 & e^{i\frac{\pi}{4}} \end{bmatrix} \tag{4}$$

In both classical and quantum computing, one of the most useful operations are the controlled operations: 'if condition A is true, perform the operation B'. Consider a system made of 2 qubits; the computational basis is defined as:

$$|0\rangle \otimes |0\rangle, |0\rangle \otimes |1\rangle, |1\rangle \otimes |0\rangle, |1\rangle \otimes |1\rangle, \text{ denoted for simplicity: } |00\rangle, |01\rangle, |10\rangle, |11\rangle \tag{5}$$

The fundamental controlled-opetation is the controlled-NOT (C-NOT) gate which action on a two-qubit system is given by $|i\rangle|j\rangle \rightarrow |i\rangle|i \oplus j\rangle$. In the computational basis, the matrix representation of the C-NOT gate is

$$\begin{bmatrix} 1 & 0 & 0 & 0 \\ 0 & 1 & 0 & 0 \\ 0 & 0 & 0 & 1 \\ 0 & 0 & 1 & 0 \end{bmatrix} \tag{6}$$

In figure 1, the circuit representation is reported. Such representation is a simple model of a quantum algorithm in which the time flows from left to right, qubits are represented by lines, and unitary operations by boxes. In this models, the generic controlled-U operation, which is a single-qubit unitary operation performed under the condition that the control qubit(s) is(are) in the 0 state, is represented by a box together with a vertical line terminating on the control qubit(s). As an example, figure 2 shows how the controlled-NOT operation can be attained from the Pauli, and Hadamard gates.
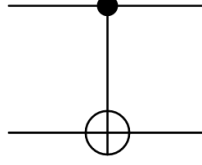
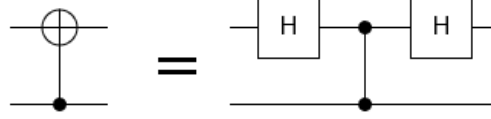Figure 1: Circuit representation of the C-NOT gate [2] (p.178)

Figure 2: C-NOT from H and C-Z [3].

In classical computing, a small set of gates (AND, OR, NOT) is sufficient to compute any function. Similarly, in quantum computation, a fundamental result states that [2] 'any unitary operation can be approximated to arbitrary accuracy using Hadamard, phase, C-NOT, and $\frac{\pi}{8}$ gates' (p.189). This set of gates is said to be universal for quantum computation.

Quantum algorithms terminate with a projective measurement. A projective measurement is described by an observable, M of the system being observed. The observable has a spectral decomposition, with respect to a particular basis,

$$M = \sum_m m P_m \tag{7}$$

where P_m is the projector onto the eigenspace of M with eigenvalue m.
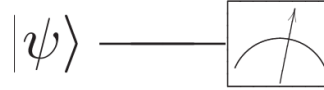

Figure 3: Circuit representation of a measurement [2] (p.186).

In the next section, one of the first discovered quantum algorithms capable of solving a specific task more efficiently than a classical computer is described.

2 The Deutch-Jozsa Algorithm

In a paper by David Deutch and Richard Jozsa published in 1992 [4], the fact that a quantum algorithm can, in principle, effectively solve a computational task faster than any other classical algorithm performed on a classical deterministic or stochastic computer is rigorously proven. The functioning of the Deutch-Jozsa algorithm is as follows.

Let $\mathcal{H}_{mn}$ be a Hilbert space of dimension mn and let

$$|i,j\rangle \; i \in \mathbf{Z}_n, j \in \mathbf{Z}_m \tag{8}$$

be a fixed orthonormal basis in $\mathcal{H}_{mn}$.

Suppose that U_f is a device (usually denoted as oracle) that computes a function $f : \mathbf{Z}_{2N} \to \mathbf{Z}_2$.

The problem to solve is the following:

find a true statement in the list

1. f is NOT a constant function

2. the sequence f(0), f(1), ... , f(2N-1) does not contain exactly N zeros (and therfore, f is not a 'balanced' funcion)

Let's first consider the classical solution: it consists of running U_f repeatedly until one of the statements is certainly true: f($\Pi(0)$), f($\Pi(1)$), ... where Π is a permutation on $\mathbf{Z}_{2N}$. It turns out that, the number of invocations of U_f, for a large number of funcions, is on average:

$$\frac{N+1}{2^{N-1}} + \sum_{n=1}^{\infty} n(\frac{1}{2})^{n-1} = 3 - \frac{1}{2^{N-1}} \approx 3 \text{ for large N} \tag{9}$$

For the quantum version of the solution, let's suppose that U_f effects the unitary operation

$$|i, j\rangle \rightarrow |i, j \oplus_m f(i)\rangle \tag{10}$$

and let S be the unitary operation that acts as

$$S |i, j\rangle = (-1)^j |i, j\rangle. \tag{11}$$

The method consists in preparing the state

$$|\phi\rangle = \frac{1}{\sqrt{2N}} \sum_{i=0}^{2N-1} |i, 0\rangle \tag{12}$$

and applying U_f, S, U_f successively to the $|\phi\rangle$ state:

$$|\phi\rangle \rightarrow |\psi\rangle \equiv \frac{1}{\sqrt{2N}} \sum_{i=0}^{2N-1} (-1)^{f(i)} |i, 0\rangle. \tag{13}$$

The magnitude of the inner product

$$|\langle\phi|\psi\rangle| = \left| \frac{1}{2N} \sum_{i=0}^{2N-1} (-1)^{f(i)} \right| \tag{14}$$

is 0 when the statement (2.) is false and 1 when statement (1). is false, thus performing the projective measurement $|\phi\rangle \langle\phi|$, the outcome tells us which statement is true. Note that the result of the measurement is either 0 or 1, therefore, this algorithm establishes the truth of 1 or 2 with certainty invoking the oracle exactly twice. To be precise, one should take into account not only the number of invocations of the oracle but also the number of steps required to solve the problem. But both choosing the permutation Π and performing the projective measurement $|\phi\rangle \langle\phi|$ requires on average $\mathcal{O}(\ln N)$ steps. Therefore a clear improvement has been achieved over the classical method.

As an example, the case N=3 is described step by step. Let U_f be the oracle that computes the function $f : \{0,1,2,3,4,5\} \rightarrow \{0,1\}$. The state $|\phi\rangle$ is prepeared as:

$$|\phi\rangle = \frac{1}{\sqrt{6}} \Big(|0, 0\rangle + |1, 0\rangle + |2, 0\rangle + |3, 0\rangle + |4, 0\rangle + |5, 0\rangle \Big), \tag{15}$$

then by appling U_f, S, U_f the state $|\psi\rangle$ is atteined:

$$U_f |\phi\rangle = \frac{1}{\sqrt{6}} \Big(|0, 0 \oplus_n f(0)\rangle + |1, 0 \oplus_n f(1)\rangle + |2, 0 \oplus_n f(2)\rangle + ...\Big), \tag{16}$$

$$SU_f |\phi\rangle = \frac{1}{\sqrt{6}} \Big((-1)^{f(0)} |0, f(0)\rangle + (-1)^{f(1)} |1, f(1)\rangle + (-1)^{f(2)} |2, f(2)\rangle + ...\Big), \tag{17}$$

$$U_f SU_f |\phi\rangle = \frac{1}{\sqrt{6}} \Big((-1)^{f(0)} |0, 0\rangle + (-1)^{f(1)} |1, 0)\rangle + (-1)^{f(2)} |2, 0\rangle + ...\Big). \tag{18}$$

The magnitude of the inner product is then

$$\left| \langle \phi | U_f S U_f | \phi \rangle \right| = \left| \frac{1}{6} \sum_{i=0}^{5} (-1)^{f(i)} \right| = 0 \text{ or } 1. \tag{19}$$

For balanced or constant funcions respectively. Although this algorithm is thought appositely to be performed faster on a quantum machine, this article is considered a milestone in the theory of quantum computation since it describes the first computational task for which a quantum processor can obtain the solution faster, with certainty and more efficiently than any classical machine.

Two years later, Peter Shor developed the famous factoring algorithm that bears his name [5], increasing the interest in the physical realizations of quantum computers.

3 Physical realizations

In a paper published in 2000, David DiVincenzo outlined five criteria required for the physical realization of quantum computers. These requirements have been used as a guide to understand whether a quantum mechanical system can be exploited to realize a quantum computer. The criteria are [6]:

1. 'A scalable physical system with well characterized qubits

2. The ability to initialize the state of the qubits to a simple fiducial state, such as $|000...\rangle$

3. Long relevant decoherence times (footnote), much longer than the gate operation time

4. A universal set of quantum gates

5. A qubit-specific measurement capability.' (pp. 2-5)

In light of these criteria, trapped-ion quantum computers represent one of the most promising ways to realize programmable QCs. The next sections will describe the state of the art of such devices. The most remarkable demonstrations of trapped-ion quantum computing are made by two independent groups: the **IonQ** company based in Maryland [7] and the Institut fur Experimentalphysik of the **University of Innsbruck** [8]. IonQ is a private company co-founded by the professors Christopher Monroe and Jungsang Kim in 2015, and since then, they have rised big foundings from different venture firms such as Google Ventures and NEA.

3.1 Linear Paul traps

In trapped-ion quantum computers, the scalable physical system with well-characterized qubits is realized by trapping ions in radiofrequency traps while storing the information in pairs of their energy levels. To do so, at the base of all these devices, there is a Paul trap which functioning is described below [9].

Earnshaw's theorem states that charged particles cannot be trapped in 3D by just electrostatic forces. Instead, a rapidly oscillating electric field with quadrupole geometry is obtained using four electrodes, as shown in figure 3.1. As a result, an oscillating potential

$$V(x, y, t) = \frac{V_0}{2} \cos{(\Omega t)}(1 + \frac{x^2 - y^2}{R^2}). \tag{20}$$

is created. While trapping multiple ions, the ion chain is aligned along the trapping axis, which is parallel to Z and passes through the quadrupole null point (x_0, y_0).

By first evaluating $\vec{E} = \vec{\nabla} V$ one finds the equations of motion:

$$F_x = eE_x = m\frac{\mathrm{d}^2 x}{\mathrm{d}t^2} = -\frac{eV}{R^2} \cos{(\Omega t)}x \ , \ x(0) = x_0 \ , \ \left. \frac{\mathrm{d}x}{\mathrm{d}t} \right|_0 = 0 \tag{21}$$

$$F_y = eE_y = m\frac{\mathrm{d}^2 y}{\mathrm{d}t^2} = -\frac{eV}{R^2} \cos{(\Omega t)}y \ , \ y(0) = y_0 \ , \ \left. \frac{\mathrm{d}y}{\mathrm{d}t} \right|_0 = 0. \tag{22}$$
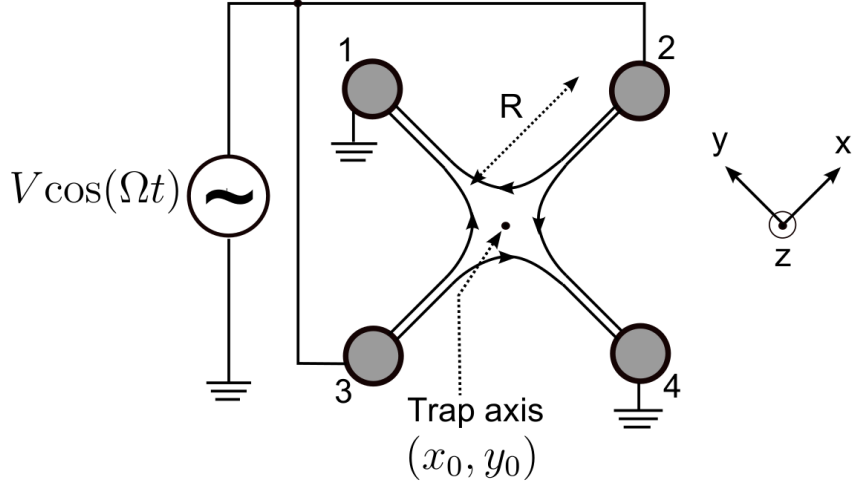
Figure 4: Linear Paul trap [10] (p.14).

Assuming that the spatial variation of the field is negligible so that $\frac{eVx}{R^2}$ can be treated as a constant one finds these expressions:

$$x(t) - x_0 = \frac{eV}{m\Omega^2 R^2} \cos{(\Omega t)}x \tag{23}$$

$$y(t) - y_0 = -\frac{eV}{m\Omega^2 R^2} \cos{(\Omega t)}y, \tag{24}$$

that plugged into the Taylor expansion of $\vec{\mathbf{F}}(x, y, t) = e\vec{\mathbf{E}}(x, y, t)$ give the force experienced by the ions in the trap:

$$\vec{\mathbf{F}} = e(E_0(x_0, y_0)\cos\Omega t - C\cos^2(\Omega t)x\hat{x} - C\cos^2(\Omega t)y\hat{y}) \tag{25}$$

where

$$C = \frac{eV}{\sqrt{2}m\Omega^2 R^4}. \tag{26}$$

By averaging over the oscillation period of the electric field the resulting force is

$$\vec{\mathbf{F}}' = -e\frac{C}{2}x\hat{x} - e\frac{C}{2}y\hat{y}, \tag{27}$$

which compared with the force involved in the classical harmonic oscillator $F(r) = -m\omega^2 r$ gives the radial so-called *secular frequency* of the trap:

$$\omega = \frac{eV}{\sqrt{2}m\Omega R^2}. \tag{28}$$

In practice, slightly different versions of the Paul trap described above are used. In some of the first IonQ processors [11, 10, 9, 12, 13], the four electrodes are segmented blades, as shown in figure 3.1 , each of the segments is driven by independent voltage sources, and by applying specific different voltages to different blades, axial confinement is achieved. In Innsbruck, the ions are confined by the use of a linear Paul trap very similar to the one described, and axial confinement is achieved by applying a static electric-field with the use of two endcaps electrodes. Some more recent demonstrations [14] instead, use surface Paul traps, which have a different geometry that allows more optical access to the ions and are, in principle, more easily scalable.
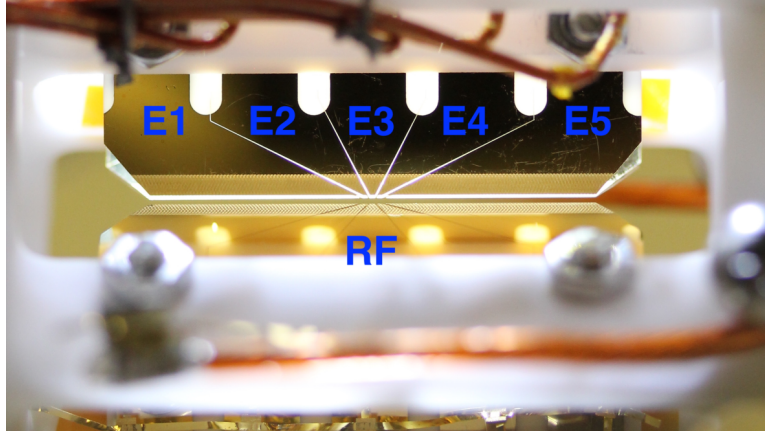
Figure 5: IonQ Paul trap with segmentet blades for axial confinement [9] (p.18).

3.2 Ions choice and state detection

There are many possible choices for the atomic ions in which valence electron states can be used to implement the qubit. Since QCs deal with positively charged ions, the Group-II or Group-II-like atoms, because of their hydrogen-like behavior, are the most suitable. In these devices, mainly two different ways of storing quantum information are used: two hyperfine or Zeeman sublevels of the ground state of the ion, or a ground state together with an optically accessible metastable excited state. Here, the characteristics of two of the most used ions, that are ^{40}Ca$^+$ and ^{171}Yb$^+$ are presented.

3.2.1 ^{40}Ca$^+$

Innsbruck University's processors [15, 16, 17] encode qubits in the $4\,^2\mathrm{S}_{\frac{1}{2}}$ ground state and the $3\,^2\mathrm{D}_{\frac{5}{2}}$ metastable state (with a natural lifetime of 1.1s) of the ^{40}Ca$^+$ ion. The $4\,^2\mathrm{S}_{\frac{1}{2}}$ state consists of two Zeeman sublevels ($m_j = \pm 1/2$) whereas the $^3\mathrm{D}_{\frac{5}{2}}$ state has six sublevels ($m_j = \pm 1/2, \pm 3/2, \pm 5/2$) and the choice is to set the computational basis as $|1\rangle \equiv \left|4\,^2\mathrm{S}_{\frac{1}{2}}, m_j = -1/2\right\rangle$ and $|0\rangle \equiv \left|^3\mathrm{D}_{\frac{5}{2}}, m_j = -1/2\right\rangle$, to take advantage of the small magnetic field dependence of this transition. Moreover, the qubit can be implemented by the two Zeeman sublevels of the $4\,^2\mathrm{S}_{\frac{1}{2}}$ ground-state, which are stable and do not spontaneously decay: $|1_z\rangle \equiv \left|4\,^2\mathrm{S}_{\frac{1}{2}}, m_j = -1/2\right\rangle$ and $|0_z\rangle \equiv \left|4\,^2\mathrm{S}_{\frac{1}{2}}, m_j = +1/2\right\rangle$.

Figure 3.2.1 shows a level scheme with all the relevant levels for both qubit encoding and state detection.
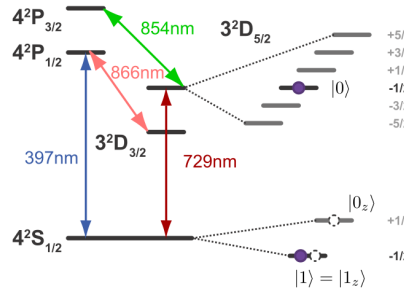

Figure 6: ^{40}Ca$^+$ relevant levels used for qubit encoding and state detection [15] (p.3).

To perform a projective measurement the $4\,\mathrm{S}_{\frac{1}{2}} \leftrightarrow 4\mathrm{P}_{\frac{1}{2}}$ transition is driven at a wavelength of 397 nm and simultaneously the resulting scattered photons collected. By driving the transition, the state is projected either into the $4\,^2\mathrm{S}_{\frac{1}{2}}$ or $3\,^2\mathrm{D}_{\frac{5}{2}}$ state. If the ion is projected in the $3\,^2\mathrm{D}_{\frac{5}{2}}$ state than it is not affected by the laser and no scattered photons are collected. If the ion is projected into the $4\,\mathrm{S}_{\frac{1}{2}}$ state then after being driven to the $4\mathrm{P}_{\frac{1}{2}}$ it can decade either back into

the $4\,\mathrm{S}_{\frac{1}{2}}$ or into the $3\,\mathrm{D}_{\frac{3}{2}}$ so that it needs to be brought back to the $4\mathrm{P}_{\frac{1}{2}}$ with light at 866 nm. These cyclic transitions are run for a sufficiently long time (100 μs) to collect enough photons.
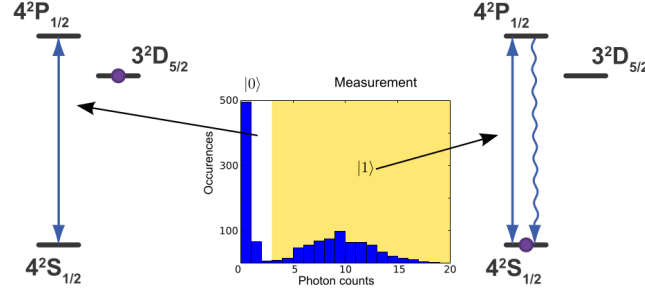

Figure 7: $^{40}\mathrm{Ca}^+$ relevant transitions used for projective measurement, the colored area illustrates the treshold wether the state is detected as $|0\rangle$ or $|1\rangle$ [15] (p.3).

3.2.2 $^{171}\mathrm{Yb}^+$

IonQ's processors [9, 10, 11, 12, 13] encode the qubit in the (F $=0$,$m_F = 0$) and the (F $=1$, $m_F =0$) hyperfine levels of the $^2\mathrm{S}_{\frac{1}{2}}$ ground state: $|0\rangle \equiv \left|^2\mathrm{S}_{\frac{1}{2}}, F = 0, m_F = 0\right\rangle$ and $|1\rangle \equiv \left|^2\mathrm{S}_{\frac{1}{2}}, F = 1, m_F = 0\right\rangle$. These states are the so-called 'clock' states because they are insensitive to magnetic field to first order: the energy splitting is $\omega = 2\pi \times 12.6428 + \delta$ GHz where $\delta = 2\pi \times 310.8B^2$ Hz with B expressed in Gauss. Furthermore, at this energy splitting, the spontaneous emission rate is virtually zero. The cyclic transition used for state detection is $\left(^2S_{\frac{1}{2}}, F = 1\right) \leftrightarrow \left(^2P_{\frac{1}{2}}, F = 0\right)$ with π and σ polarization elements added to ensure cycling (there is a small branching ratio of 0.5% to the transition $^3\mathrm{D}_{\frac{3}{2}}$ that must be taken into account) from all of the Zeeman levels in the $\left(^2S_{\frac{1}{2}}, F = 1\right)$. If the ion is projected into the $|0\rangle$ state then no photons are scattered, vice versa, if the state is projected into the $|1\rangle$ then photons are scattered and collected. Again, these cyclic transitions are run for a sufficiently long time to collect enough photons.
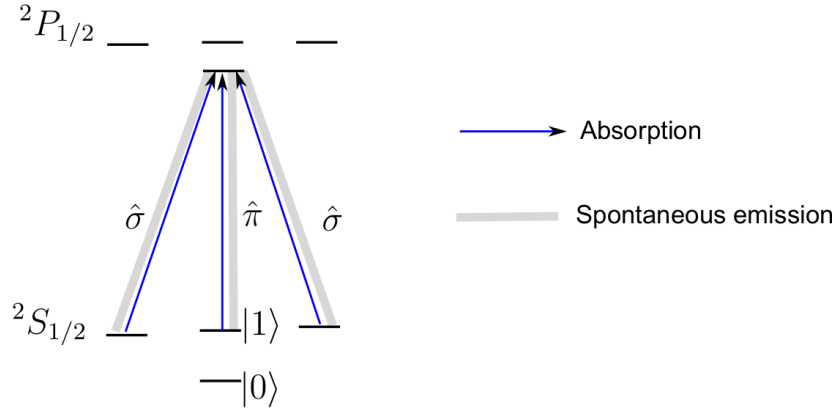

Figure 8: $^{171}\mathrm{Yb}^+$ relevant energy levels and transitions for state detection [10] (p.31).

3.3 Laser cooling and state inizialization

Once loaded, the ions need to be initialized: the qubit state of each ion is prepared in a definite state (usually $|0\rangle$), and the motional state of the ion string is cooled down, from its high temperature, to near the ground state. The initialization of the qubit register is made possible by the technique of optical pumping, while the motional state of the chain is Doppler cooled to a mean phonon number $\langle n \rangle \approx 10$ and then sideband cooled to near the motional ground state.

3.3.1 Doppler cooling

The first stage of the laser cooling is the Doppler cooling, a technique that was first proposed by Hänsch and Schawlow [18] in 1975.

It is performed by first making the ion continuously scattering light using a laser resonant with the desired optical transition and then red-detuning its frequency. In the ^{171}Yb$^+$ case [9] this means decreasing the laser frequency of the 369.5 nm transition between $\left(^2S_{\frac{1}{2}}, F = 1\right)$ and $\left(^2P_{\frac{1}{2}}, F = 0\right)$. The scattering rate Γ in this situation can be written as:

$$\Gamma = \frac{s\frac{L}{2}}{1 + s + 4\frac{\Delta^2}{L^2}}, \tag{29}$$

where L is the radiative linewidth of the decay from the excited state, and s depends on the lifetime of the excited state and the wavelenght of the light. Δ is the detuning of the excitation laser frequency from resonance. For the vibrating ion one can write $\Delta = \delta - \vec{k} \cdot \vec{v}$ where δ is the detuning from resonance, $\vec{v}$ is the velocity of the ion, $\vec{k}$ is the k-vector of the scattered photon and $\vec{k} \cdot \vec{v}$ is then the first order Doppler shift experienced by the ion. It is clear how the scattering rate increases while the ion is travelling towards the photon since the Doppler shift is negative. Due to the fact that the following spontaneous emissions are isotropic with both π and σ polarizations emitted, the effect of these emissions averages to zero and the net result of this process is the ion reducing its momentum by $\hbar k$ in the $\hat{k}$ direction.
Quantitatively, for what regards the trapped ^{171}Yb$^+$ ions of the IonQ's QCs [9, 10, 11], to cool down the motional state, the laser detuning δ ranges from about $-2\pi \times 300$ MHz for initial high kinetic energy to $-2\pi \times 10$ MHz.

3.3.2 Optical pumping

To briefly describe how the ion qubits are initialized to the desired state by optical pumping, let's consider again the ^{171}Yb$^+$ case [11]: to initialize the ion in the state $|0\rangle \equiv \left|^2S_{\frac{1}{2}}, F = 0, m_F = 0\right\rangle$ a beam that is resonant to the transitions between the F=1 states in the S manifold and the F=1 states in the P manifold is applied with all polarizations as schematized in figure 3.3.2. The F=1 state in the P manifold can either decay back to the F=1 state of the S manifold, and therefore be pumped back to P, or to the sought $|0\rangle$ state, that is 12.6 GHz detuned from the F=1 state of the same manifold.
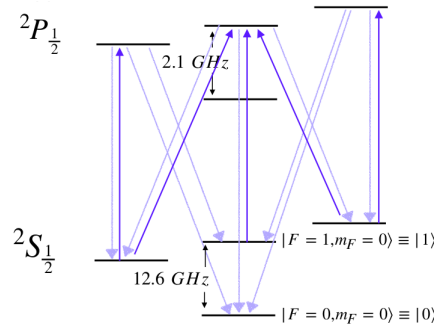

Figure 9: ^{171}Yb$^+$ transitions for state initialization by optical pumping [9] (p.24).

4 Coherent control of qubits

Once the ions are loaded and cooled down, and the qubits are initialized to the $|0\rangle$ state, to perform the algorithm, a chain of operations is used in order to translate the desired quantum gates to gates native to the hardware level of the machine. An entangling gate together with single-qubit operations forms a universal set of gates. The first proposed way to realize an entangling gate on trapped ions was made by I. Cirac and P. Zoller in 1994 [19]. In 2003 at the Univerity of Innsbruck, the first CNOT quantum gate implemented according to their proposal was realized [20]. The Cirac-Zoller gate works exploiting the common vibration of the ion string

to mediate the interaction between the qubits. In current trapped-ions programmable QCs, quantum gates are based on the idea of Mølmer and Sørensen [21]. Their gate, unlike the Cirac-Zoller one, has the advantage that the motional state of the ions need not be cooled down completely to ground state.

4.1 Single qubit rotation

A qubit superposition state $|\psi\rangle = cos\theta\,|0\rangle + e^{i\phi}\sin\theta\,|1\rangle$ can be represented as a point on the surface of a sphere known as the Bloch sphere. Rotations of an angle θ about an axis described by the azimuthal angle ϕ in the XY plane are represented by the unitary matrices

$$R(\theta, \phi) = \begin{bmatrix} \cos\frac{\theta}{2} & -ie^{-i\phi}\sin\frac{\theta}{2} \\ -ie^{i\phi}\sin\frac{\theta}{2} & \cos\frac{\theta}{2} \end{bmatrix}. \tag{30}$$

These rotations can be attained by applying a Raman pulse with a controlled duration and a controlled phase. What follows is the general theory of these stimulated Raman transitions used to implement single-qubit rotations.

$$|q\rangle \boxed{H} \quad = \quad \boxed{R_{\mathrm{y}}\!\left(\tfrac{\pi}{2}\right)} \boxed{R_{\mathrm{x}}(\pi)} \quad = \quad \boxed{R_{\mathrm{z}}(\pi)} \boxed{R_{\mathrm{y}}\!\left(\tfrac{\pi}{2}\right)}$$

Figure 10: Hadamard gate implementation using rotations: rotations about the x-axis ($R_x(\theta)$) and rotations about the y-axis ($R_y(\theta)$) can be atteined by setting $\phi = 0$ and $\phi = \frac{\pi}{2}$ respectively. Rotations about the z-axis ($R_z(\theta)$) can be constructed from three rotations about axes in the xy plane [11] (p.80).

4.2 Raman transitions

Let's consider the-three level system $|0\rangle$, $|1\rangle$, $|2\rangle$ composed by the two qubit states and an energetically higher one [22]. The aim is to coherently drive transitions between $|0\rangle$ and $|1\rangle$ using $|2\rangle$ as an intermediate state. This is obtained using two lasers, both detuned from the intermediate state to avoid driving population into it. Fugure 4.2 shows the relevant energy levels and laser detunings: δ is the detuning from the two-photon resonance frequency, and it is taken to be much smaller than the detuning Δ of the lasers from the auxiliary state.
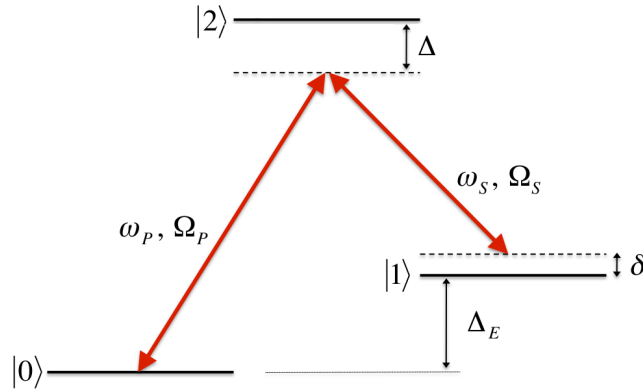

Figure 11: Relevant energy levels and detunings for Raman transition [22] (p.13).

In the basis $\{|0\rangle, |1\rangle, |2\rangle\}$, in the rotating wave approximation, the Hamiltonian of the system is

$$\hat{H} = \begin{pmatrix} 0 & 0 & \Omega_p \\ 0 & -2\delta & \Omega_S \\ \Omega_p & \Omega_S & -2\Delta \end{pmatrix}, \tag{31}$$

where Ω_p and Ω_S are the Rabi frequencies of the lasers given by the expectation values of the dipole transition operator $\hat{D}$ and the laser amplitude $\vec{\mathbf{E}}_{p,S}$:

$$\begin{aligned} \Omega_p &= -\frac{1}{\hbar} \langle 2| \hat{D} \cdot \vec{\mathbf{E}}_p |0\rangle \\ \Omega_S &= -\frac{1}{\hbar} \langle 2| \hat{D} \cdot \vec{\mathbf{E}}_S |1\rangle \end{aligned} \tag{32}$$

The time-dependent Schrödinger equation

$$\hat{H} |\psi(t)\rangle = i\hbar \frac{\mathrm{d}}{\mathrm{d}t} |\psi(t)\rangle \tag{33}$$

with

$$|\psi(t)\rangle = c_0(t) |0\rangle + c_1(t) |1\rangle + c_2(t) |2\rangle \tag{34}$$

gives three coupled equations for the time-dependent coefficients $c_i(t)$:

$$\begin{aligned} i\frac{\mathrm{d}}{\mathrm{d}t}c_0(t) &= \frac{1}{2}\Omega_p c_2(t) \\ i\frac{\mathrm{d}}{\mathrm{d}t}c_1(t) &= \frac{1}{2}\Omega_S c_2(t) - \delta c_1(t) \\ i\frac{\mathrm{d}}{\mathrm{d}t}c_2(t) &= \frac{1}{2}(\Omega_p c_0(t) + \Omega_S c_1(t)) - \Delta c_2(t). \end{aligned} \tag{35}$$

If the detuning is much greater than the Rabi frequencies, then the population in $|2\rangle$ will oscillate fast and $\frac{\mathrm{d}}{\mathrm{d}t}c_2(t)$ will average out to zero so the system can be reduced effectively to a two-level system. By substituting $c_2(t) = \frac{1}{2\Delta}(\Omega_p c_0(t) + \Omega_S c_1(t))$ into the first two equations one obtains:

$$i\hbar \frac{\mathrm{d}}{\mathrm{d}t} |\bar{\psi}(t)\rangle = \hat{H}_{eff} |\bar{\psi}(t)\rangle \tag{36}$$

with

$$\begin{aligned} |\bar{\psi}(t)\rangle &= c_0(t) |0\rangle + c_1(t) |1\rangle \\ \hat{H}_{eff} &= \frac{\hbar}{4} \begin{pmatrix} \frac{\Omega_p^2}{\Delta} & \frac{\Omega_p \Omega_S}{\Delta} \\ \frac{\Omega_p \Omega_S}{\Delta} & \frac{\Omega_S^2}{\Delta} - 4\delta \end{pmatrix} \end{aligned} \tag{37}$$

The two diagonal terms are known as Stark shifts: they are energy shifts of the $|0\rangle$ and $|1\rangle$ states of $\hbar\frac{\Omega_p^2}{4\Delta}$ and $\hbar\frac{\Omega_S^2}{4\Delta}$ respectively. Due to these shifts, the effective two-photon Raman detuning is now

$$\delta_{eff} = \delta - (\hbar\frac{\Omega_S^2}{4\Delta} - \hbar\frac{\Omega_p^2}{4\Delta}) \tag{38}$$

In conclusion, by solving explicitly the time-dependent Schrödinger equation 36 and assuming that at t=0 the population is in the $|0\rangle$ state, one finds the time-dependent coefficients of the superposition of the stationary states:

$$\begin{aligned} |c_0(t)|^2 &= 1 + \frac{\Omega_R^2}{2\Omega_0^2}(\cos\Omega_0 t - 1), \\ |c_1(t)|^2 &= \frac{\Omega_R^2}{2\Omega_0^2}(1 - \cos\Omega_0 t), \end{aligned} \tag{39}$$

with

$$\Omega_R = \frac{\Omega_p \Omega_S}{2\Delta}$$
$$\Omega_0 = \sqrt{\Omega_R^2 + \delta_{eff}^2}.$$

(40)

Note that to transfer all population to $|1\rangle$, which means perturbing the system for $t_\pi = \frac{\pi}{\Omega_0} s$ (known as the π time) obtaining $|c_1|^2 = 1$, is possible only when $\delta_{eff} = 0$. In the experiments described here, rotation fidelities of 98-99 % have been achieved [11, 12].

5   Mølmer and Sørensen gate

In their paper [21], Mølmer and Sørensen, presented an alternative implementation to that of Cirac and Zoller [19] for which the vibrational state need not be cooled down near the ground state. Both the Cirac-Zoller and Mølmer-Sørensen (MS) gates, tough, use collective spatial vibrational modes for communication between ions. These vibrational modes result from the (approximately) quadratic potential to which ions are subject, and to their mutual Coulomb interaction. The potential energy of the N-ion string is then:

$$V = \sum_{i=1}^{N} \frac{1}{2} M\omega^2 x_i(t)^2 + \sum_{\substack{i,j=1 \\ i \neq j}}^{N} \frac{Z^2 e^2}{8\pi\epsilon_0} \frac{1}{|x_i(t)^2 - x_j(t)^2|},$$

(41)

where ω is the trap frequency as defined in equation 28, Z is the total charge of the ion, e is the electron charge an ϵ_0 is the permittivity of free space. For small oscillations from the equilibrium, the mode frequencies and the way each ion participates in each mode of motion, can be obtained respectively by (numerically) finding the eigenvalues and the eigenvectors of the matrix $\frac{\partial^2 V}{\partial x_i \partial x_j}$ evaluated at the equilibrium point.

The MS two-qubit quantum gate is performed by coupling the states

$$|ggn\rangle \leftrightarrow \{|eg(n+1)\rangle, \ |ge(n-1)\rangle\} \leftrightarrow |een\rangle,$$

where g, e denotes the internal state of the ions, and the third letter is the quantum number for the significant vibrational mode. The coupling is attained by addressing the first ion with a laser with detuning δ from the resonance with a joint motional and internal excitation of the ion. The second ion is addressed by another laser with detuning $-\delta$ (figure 5). The detuning is chosen to be sufficiently large so that the intermediate states are not populated, but sufficiently small to neglect all other vibrational modes.
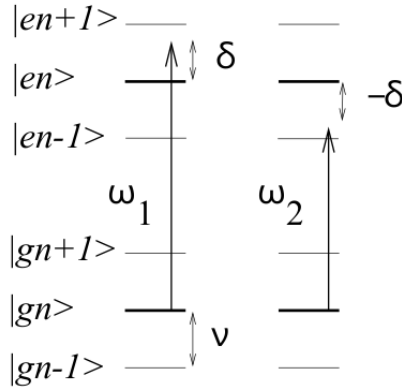

Figure 12: Laser detuning for the two ions [21] (p.4).

Mathematically, the system is described by the Hamiltonian

$$H = H_0 + H_{int}$$

$$H_0 = \hbar\nu(a^\dagger a + \frac{1}{2}) + \hbar\omega_{eg}\sum_j \frac{\sigma_{zj}}{2}$$

$$H_{int} = \sum_j \frac{\hbar\Omega}{2}(\sigma_{+j}e^{i(\eta(a+a^\dagger)-\omega_j)} + h.c.),$$

(42)

where ν is the frequency of the relevant vibrational mode, a and $a^\dagger$ are the ladder operators of the harmonic oscillator, $\hbar\omega_{eg}$ is the energy difference between $|e\rangle$ and $|g\rangle$, ω_j is the frequency of the laser addressing the j-th ion, σ_{zj} and σ_{+j} are the z Pauli operator and the rising operator respectively, which represent the two internal degrees of freedom of the j-th ion. Furthermore, it has been assumed that for both the Lamb-Dicke parameter η_j and the Rabi frequency of the lasers Ω_j, one has $\eta_1 = \eta_2 = \eta$ and $\Omega_2 = \Omega_2 = \Omega$.

In this situation, the only energy conserving transition is between $|ggn\rangle$ and $|een\rangle$. The Rabi frequency for this transition can be determined by second order perturbation theory:

$$\tilde{\Omega} = \frac{2}{\hbar}\sum_m \frac{\langle een|H_{int}|m\rangle\langle m|H_{int}|ggn\rangle}{E_m - (E_{ggn} + \hbar\omega_m)},$$

(43)

where the sum is over $|m\rangle = |eg(n+1)\rangle,\ |ge(n-1)\rangle$, E_m is the energy of the unperturbed state $|m\rangle$ and ω_m is the frequency of the laser exciting the $|m\rangle$ state. If the ion trap is operating in the Lamb-Dicke limit, i.e. the value of $\eta\sqrt{n+1}$ is well below unity, the exponentials can be expanded as $e^{\eta(a+a^\dagger)} \approx 1 + \eta(a+a^\dagger)$ and the Rabi frequency for the transition is

$$\tilde{\Omega} = -\frac{(\Omega\eta)^2}{\nu - \delta}$$

(44)

where $\delta = \omega_1 - \omega_{eg}$ is the detuning of the laser addressing the first ion. The Rabi frequency remarkably does not depend on the quantum number n. As a result, the population of the internal states $|gg\rangle$ and $|ee\rangle$ oscillates sinusoidally. In figure 5 the numerically computed evolution of the density matrix elements $\rho_{ijlm}|ij\rangle\langle lm|$, where $i,j,l,m = e,g$, is reported.
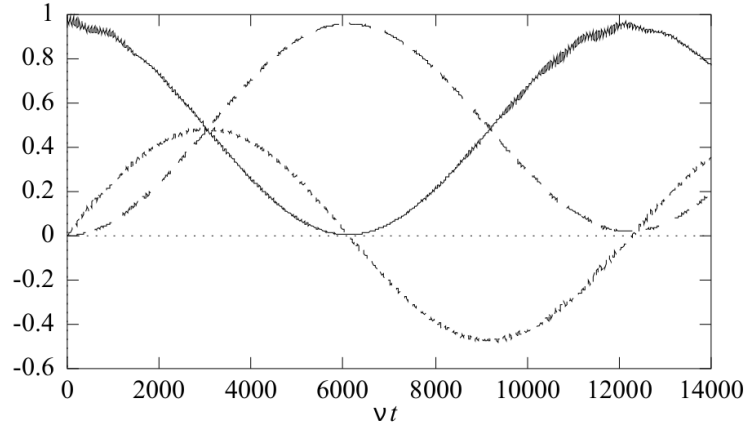

Figure 13: Rabi oscillations between $|gg\rangle |ee\rangle$. The first curve (counting from above at $\nu t \approx$ 2000) is ρ_{gggg}, the second is $\text{Im}\{\rho_{gggg}\}$ and the third is ρ_{eeee}. Parameters are $\delta = 0.90\nu$, $\Omega = 0.10\nu$ and $\eta = 0.10$. The mean excitation of the vibrational state is $\bar{n} = 2$ [21] (p.4).

For what seen so far, starting from the state $|gg\rangle$, by applying a radiation field pulse of the duration of $\frac{\pi}{2\tilde{\Omega}}$ the maximally entangled state $\frac{1}{\sqrt{2}}(|gg\rangle - i|ee\rangle)$ (the EPR-state) can be obtained. This entangling operation, together with signle-qubit rotations, forms a universal set of gates from which any unitary operation can be attained. In the next section, an example of how single-qubit and two-qubit gates are used in practice to implement the Deutsch–Jozsa algorithm is presented.

6 Implementation of the Deutsch–Jozsa algorithm

In this section, the demonstration made by C. Monroe et at [12] of how a small programmable quantum computer with atomic qubits can implement the Deutsch-Jozsa algorithm [4] is presented. The processor used consists of trapped ^{171}Yb$^+$ with the hyperfine states choosen as computational basis as described in section 3.2.2. The ions are laser-cooled to near their motional groud states and initialized to $|0\rangle$ by optical pumping. Measurements are performed by driving the cyclic transitions described in section 3.2.2 and collecting the state-dependence fluorescence. At the lowest leve, quantum gates are single qubit rotations and two-qubit XX-gates atteined as described in the previous sections. Single qubit rotations are of the form of equation 30 and the rotations relevant for the Deutsch-Jozsa algorithm are

$$R_{\pm y}(\frac{\pi}{2}) = R(\pm\frac{\pi}{2}, \frac{\pi}{2}),$$
$$R_x(\frac{\pi}{2}) = R(0, \frac{\pi}{2}), \tag{45}$$
$$R_z(\frac{\pi}{2}) = R_y(-\frac{\pi}{2})R_x(\frac{\pi}{2})R_y(\frac{\pi}{2}).$$

The XX-gate, in the computational basis, is represented by

$$\begin{bmatrix} 1 & 0 & 0 & \pm i \\ 0 & 1 & \pm i & 0 \\ 0 & \pm i & 1 & 0 \\ \pm i & 0 & 0 & 1 \end{bmatrix} \tag{46}$$

where the $\pm$ signs depend on how the particular two ions, on which the gate is applied, are coupled to the motional modes. From this gate it is possible to obtain the CNOT gate as shown in figure 6.
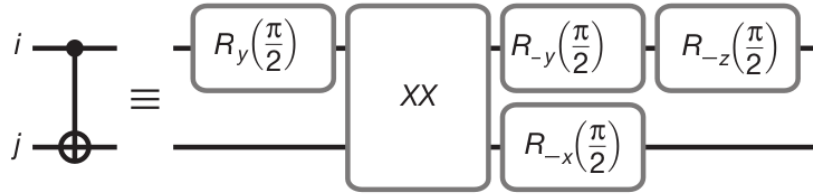

Figure 14: CNOT gate from XX gate and single-qubit rotations [12] (p.64)

The task of the algorithm, as described in section 2, is to determine whether a function is constant or balanced. In this demonstration the algorithm is performed using five qubits, denoted $X_1X_2X_3X_4X_5$, and the function to be tested acts on $n = 3$ of the five qubits: $f : \{0, 1, 2, 3, 4, 5, 6, 7(= 2^n - 1)\} \rightarrow \{0, 1\}$. The oracle that implements a balanced function is programmed by using sequences of CNOT while the oracle that implements the constant function is programmed by simply setting the fourth qubit to $|0\rangle$ or $|1\rangle$.

The algorithm is performed with all the five qubits initialized in the $|0\rangle$ state. The first step is to prepare an equal superposition of all the classical inputs of the function:

$$|\psi\rangle_1 = \frac{1}{\sqrt{8}} \sum_{i=0}^{7} |i\rangle_{123} \otimes |0\rangle_4 \otimes \frac{|0\rangle_5 + |1\rangle_5}{\sqrt{2}} \tag{47}$$

where $|i\rangle_{123}$ is the decimal representation of $|l\rangle_1 \otimes |m\rangle_2 \otimes |n\rangle_3$ with $i = l \times 2^0 + m \times 2^1 + n \times 2^2$, $l, m, n = 0, 1$.

The next step is to write the output value of the function in the fourth qubit by applying the function on the superposition of $X_1X_2X_3$. The resulting state is

$$|\psi\rangle_2 = \frac{1}{\sqrt{8}} \sum_{i=0}^{7} |i\rangle_{123} |f(i)\rangle_4 \otimes \frac{|0\rangle_5 + |1\rangle_5}{\sqrt{2}} \tag{48}$$

14

The third step is to perform a CNOT on $|f(i)\rangle_4 \otimes \frac{|0\rangle_5 + |1\rangle_5}{\sqrt{2}}$ to obtain the state

$$|\psi\rangle_3 = \frac{1}{\sqrt{8}} \sum_{i=0}^{7} (-1)^{f(i)} |i\rangle_{123} |f(i)\rangle_4 \otimes \frac{|0\rangle_5 + |1\rangle_5}{\sqrt{2}} \tag{49}$$

The last step before measurement is to perform a single-qubit rotation $R_y(\frac{\pi}{2})$ on all qubits. The measure is then performed on the first 4 qubits. Before measurement, the qubits are in the state

$$|\psi\rangle_4 = \frac{1}{8} \sum_{j=0}^{7} \sum_{i=0}^{7} (-1)^{f(i)} (-1)^{\bar{j}x} |\bar{j}\rangle_{123} \otimes \frac{|0\rangle_4 + (-1)^{f(i)} |1\rangle_4}{\sqrt{2}} \tag{50}$$

where $\bar{j}$ is the bit-wise inversion of j (e.g. $\bar{5} = 1\bar{0}1 = 010 = 2$).

Let's consider the coefficients C_{1110} and C_{1111} of the basis states $|1110\rangle$ and $|1111\rangle$. If the function is NOT balanced then

$$C_{1110} = \frac{(-1)^{f(\cdot)}}{\sqrt{2}}$$
$$C_{1111} = \frac{1}{\sqrt{2}} \tag{51}$$

vice versa, when the function is balanced

$$C_{1110} = \frac{1}{\sqrt{2}}$$
$$C_{1111} = 0. \tag{52}$$

Therefore, conditioned upon $X_4 = 1$, the outcome of the measure of $X_1 X_2 X_3$ is certain to give 111 for a constant function. For any other outcome, the function is certainly balanced.

7   Conclusion

This demonstration, together with many others [14, 16, 17], proves the versatility of the trapped-ion quantum computers. As outlined by DiVincenzo [6], two of the characteristics that make a quantum system a good quantum computer are the scalability and the ability to menage errors. Trapped-ion architectures lend themselves well to be scaled. In single linear arrays of ions, however, the speed of gates and their fidelty decreases when the number of ions grows. This is due to the weaker coupling to the ion motions resulting from the small Lamb-Dicke parameter of large mass chains. One of the most promising ways to overcome these issues is to use a system of several small chains capable of moving quantum information between them by moving the ions themselves. Trasport and separation of ions into multizone Paul traps has been recently demonstrated [23].

Errors result from two mechanisms: decoherence and imperfect control fields. The former is due to the coupling of the qubit with the environment whether the latter results from miscalibrated or noisy amplitude, frequency or polarization. Scaling and error mitigation are indeed the two big challenges the research is facing.

Trapped ions have remained one of the leading qubit technologies since quantum computing had been theorized less than three decades ago, and likely, they will remain a useful means to investigate capabilities and limitations of quantum computing.

References

[1] Deutsch D. Quantum theory, the Church–Turing principle and the universal quantum computer. Proceedings of the Royal Society of London A Mathematical and Physical Sciences. 1985;400(1818):97–117.

[2] Nielsen MA, Chuang I. Quantum computation and quantum information. AAPT; 2002.

[3] Gidney C. Breaking Down the Quantum Swap; 2020. algassert.com/post/1717.

[4] Deutsch D, Jozsa R. Rapid solution of problems by quantum computation. Proceedings of the Royal Society of London Series A: Mathematical and Physical Sciences. 1992;439(1907):553–558.

[5] Shor PW. Algorithms for quantum computation: Discrete logarithms and factoring. In: Proceedings 35th annual symposium on foundations of computer science. Ieee; 1994. p. 124–134.

[6] DiVincenzo DP. The physical implementation of quantum computation. Fortschritte der Physik: Progress of Physics. 2000;48(9-11):771–783.

[7] Monroe C, J K. IonQ; 2020. ionq.com.

[8] Blatt et al R. Institut fur Experimentalphysik; 2020. www.uibk.ac.at/exphys/index.html.de.

[9] Landsman KA. CONSTRUCTION, OPTIMIZATION, AND APPLICATIONS OF A SMALL TRAPPED-ION QUANTUM COMPUTER; 2019.

[10] Debnath S. A programmable five qubit quantum computer using trapped atomic ions. University of Maryland, College Park; 2016.

[11] Figgatt C. Building and Programming a Universal Ion Trap Quantum Computer. University of Maryland, College Park; 2018.

[12] Debnath S, Linke NM, Figgatt C, Landsman KA, Wright K, Monroe C. Demonstration of a small programmable quantum computer with atomic qubits. Nature. 2016;536(7614):63.

[13] Figgatt C, Maslov D, Landsman K, Linke NM, Debnath S, Monroe C. Complete 3-qubit Grover search on a programmable quantum computer. Nature communications. 2017;8(1):1918.

[14] Wright K, Beck K, Debnath S, Amini J, Nam Y, Grzesiak N, et al. Benchmarking an 11-qubit quantum computer. arXiv preprint arXiv:190308181. 2019;.

[15] Schindler P, Nigg D, Monz T, Barreiro JT, Martinez E, Wang SX, et al. A quantum information processor with trapped ions. New Journal of Physics. 2013;15(12):123012.

[16] Gulde S, Riebe M, Lancaster GP, Becher C, Eschner J, Häffner H, et al. Implementation of the Deutsch–Jozsa algorithm on an ion-trap quantum computer. Nature. 2003;421(6918):48.

[17] Monz T, Nigg D, Martinez EA, Brandl MF, Schindler P, Rines R, et al. Realization of a scalable Shor algorithm. Science. 2016;351(6277):1068–1070.

[18] Hänsch TW, Schawlow AL. Cooling of gases by laser radiation. Optics Communications. 1975;13(1):68–69.

[19] Cirac JI, Zoller P. Quantum computations with cold trapped ions. Physical review letters. 1995;74(20):4091.

[20] Schmidt-Kaler F, Häffner H, Riebe M, Gulde S, Lancaster GP, Deuschle T, et al. Realization of the Cirac–Zoller controlled-NOT quantum gate. Nature. 2003;422(6930):408.

[21] Sørensen A, Mølmer K. Quantum computation with ions in thermal motion. Physical review letters. 1999;82(9):1971.

[22] Hubert T. Stimulated Raman Transitions Between Hyperfine Ground States of Magnetically Trapped Rubidium-87 Atoms. Master's thesis, University of Amsterdam, Netherlands; 2015.

[23] Bowler R, Gaebler J, Lin Y, Tan TR, Hanneke D, Jost JD, et al. Coherent diabatic ion transport and separation in a multizone trap array. Physical review letters. 2012;109(8):080502.